Computational Fluid Dynamics JOURNAL vol.5. no.1 April 1996 (pp.107–128)

NUMERICAL ANALYSIS OF THREE-DIMENSIONAL TURBULENT STRUCTURE IN A SQUARE-SECTIONED 180 DEG BEND

Hitoshi SUGIYAMA† Mitsunobu AKIYAMA†
Kazunori YAMANAKA‡ Takayuki SATO♯

Abstract

Numerical simulation has been performed on developing turbulent flows through a square-sectioned duct with 180 deg bend. The ratio of the mean radius of curvature of the bend to the hydraulic diameter is 3.35 and the straight ducts of 31 hydraulic diameter long are attached to both of the inlet and outlet of the bend. In calculation, algebraic Reynolds stress model and boundary-fitted coordinate system, which were used previously by the authors [H.Sugiyama, *et al.*; CFD Journal, vol.4 pp.59–78, and also vol.4 pp.239–264], were applied. Calculated results are compared with the experimental data available [A.Melling, *et al.*; J.F.M., vol.78 pp.289–315, and S.M.Chang, *et al.*; PHC Physico Chemical Hydrodynamics, vol.4 pp.243–269].

The transition between the secondary flow of the second kind to that of the first kind was examined. In the straight duct of the inlet, secondary flow of the second kind transforms into that of the first kind at 1.0∼1.6 hydraulic diameter upstream from the bend inlet. Contrary, in the straight duct of the outlet, the secondary flow of the first kind is accelerated downstream from the bend outlet, and the secondary flow of the first kind decays gradually and transforms into the secondary flow of the second kind.

Concerning to the flow in the bend, the mean flow velocity distribution with a minimum at 90 deg bend section and the sharp spike in the streamwise velocity fluctuations near the symmetry plane at 90 deg section were successfully simulated.

1. INTRODUCTION

Curved ducts with a square cross-section are widely used as a mechanical element in many engineering systems, such as centrifugal pumps, nuclear-reactor channels, aircraft intakes and cooling coils of heat exchanger. Flows in such engineering applications are often turbulent. A characteristic feature of the curved ducts which distinguishes them from the straight ducts is the generation of streamwise vorticity or secondary motion, which is called the secondary flow of the first kind and increases pressure gradient within the curved duct. On the other hand, turbulence-driven secondary motion, which is called the secondary flow of the second

Received on February 8, 1995.

† Department of Mechanical Systems Engineering, Utsunomiya University; 2753 Ishii-cho, Utsunomiya, 321 Japan
‡ Hitachi Co.,Ltd.; 1-1,Saiwai-cho 3-chome, Hitachi-shi, 317 Japan
♯ Kao Co., Ltd.; 2606, Akabane, Ichikai-machi, Haga, 321-34 Japan

kind, has been mainly observed in non-circular straight duct. Melling and Whitelaw [1] have conducted a detailed experimental study of developing turbulent flow in a square duct by using a laser-Doppler anemometer at a Reynolds number based on the bulk velocity and the hydraulic diameter of 4.2×10^4. In their study, contours of axial mean velocity and turbulence intensity were measured in the developing flow, and three mean velocity components and five of the six Reynolds stresses were obtained in the nearly fully developed flow which corresponds to the 36.8 hydraulic diameters downstream from the duct inlet, and the vector diagram of the secondary flow of the second kind were shown. Although the strength of turbulence-driven secondary flows is only of the order of 2~3 % of the streamwise bulk velocity, this flow can have important consequence. Therefore, when the straight ducts with square cross-section are attached to both of the inlet and outlet of the curved duct, the flow behavior of such duct may become more complicated than the flow in the curved duct without straight duct. It can be said that the transition from the secondary flow of the second kind to that of the first kind and vice versa may play a role near the inlet and the outlet, respectively.

In the experimental analysis of turbulent flow in 90 deg bend of 2.3 radius ratio with long upstream and downstream straight ducts, measurements of the streamwise and radial components of the mean velocity and the corresponding components of the Reynolds stress were obtained with a laser-Doppler anemometer in various cross sections by Humphrey, *et al.* [2]. They reported that the secondary mean velocity driven mainly by the pressure gradient attains a value up to 28 % of the bulk velocity and may be largely responsible for the convection of Reynolds stresses in the cross-stream plane.

Taylor, *et al.* [3] measured flow fields in a square-sectioned 90 deg bend with 2.3 radius ratio using laser-Doppler velocimetry at Reynolds numbers of 790 and 40,000 in order to make clear the effect of inlet boundary layer on the developing turbulent flow. They reported that the boundary layer thickness at the bend inlet is influential to the flow development, particularly so when it is reduced to 0.15 of the hydraulic diameter by comparing with the fully developed inlet flow.

Chang, *et al.* [4] have measured the developing turbulent flow of 180 deg curved duct with straight ducts of 31 times hydraulic diameter long at the inlet and the outlet using non-intrusive laser Doppler velocimetry technique. They have provided detailed experimental data of the development of a turbulent flow around curved channel with the bend radius equal to 3.35 times the hydraulic diameter of the duct. Their experimental result shows that a large "hole" develops in the streamwise velocity towards the inside of the bend at 90 deg into the bend.

In numerical analysis of turbulent flow in a square-sectioned 180 deg bend, Choi [5] have tried to simulate such large "hole" [4] by adopting $k-\epsilon$ turbulence model and algebraic Reynolds stress model(ASM) in vain.

Sotiropoulos and Patel [6] also have predicted the same experimental data, evaluating three kinds of near-wall turbulent models. The comparisons between both results reveal that the full Reynolds stress model presented by Launder and Shima [7] yield much improved predictions over the two-layer $k-\epsilon$ model but fail to predict the large "hole" in streamwise velocity at 90 deg and point to the need for further refinements for more accurate representation of curvature effects.

Further discussions on the turbulence models were described in Gibson, *et al.* [17] and Akiyama, *et al.* [18]. Several benchmark test based on commercial software were also reported in [19] and [20].

Considering information about curved duct with square cross-section, we have carried out the numerical study for a developing turbulent flow in a curved duct for the purpose of making the turbulent structure clear. The well documented experiment of Chan, *et al.* [4] in turbulent flow through a strongly curved 180 deg bend of square cross-section with inlet and outlet straight ducts is selected as our numerical test case. Although this particular flow has already been computed by several researchers [5, 6] employing a wide range of turbulence closure, including high Reynolds number $k-\epsilon$ turbulence models with wall function, two-layer $k-\epsilon$ turbulence model and algebraic Reynolds stress model, to our knowledge, we can not find any reports described about the transition from the secondary flow of the second kind to that of the first kind and vice versa near the inlet and outlet of the curved duct. Therefore, this phenomenon of transition is numerically examined simultaneously with the comparison between the calculated results and the experimental data in order to make the behavior of the secondary flow clear.

Furthermore, although Reynolds number and location from the inlet are different each other, the calculated results of inlet straight duct are compared with the experimental data measured by Melling, *et al.* [1] in order to confirm the validity of the present method in developing turbulent flow of a square duct.

2. TECHNIQUE OF ANALYSIS

2.1 Subject of Numerical Analysis

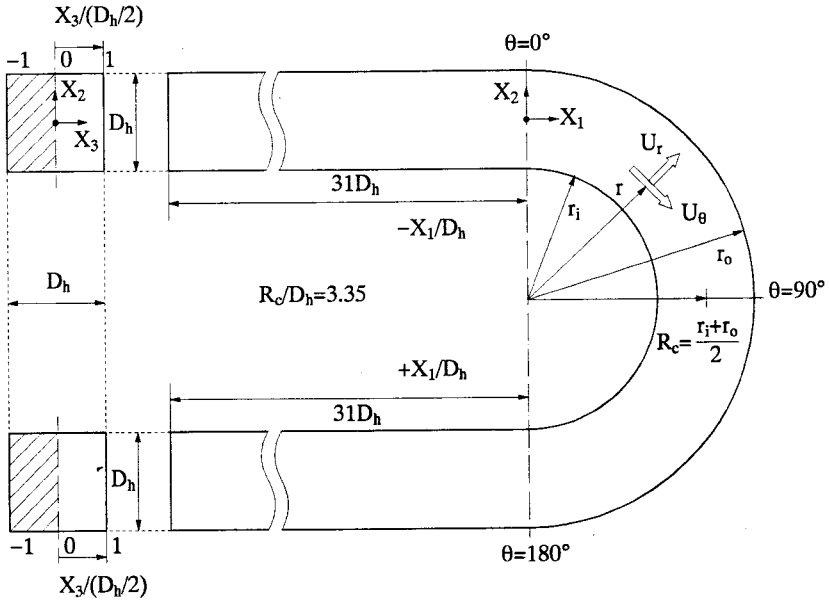

Fig.1: Subject of calculation and coordinate system

In numerical analysis, the experimental data measured in detail by Chang, *et al.* [4] was selected as a subject of calculation. Figure 1 shows a schematic diagram of the experimental apparatus and the coordinate system set in square-sectioned 180 deg bend. The flow cross-section was $4.45\times4.45\,\mathrm{cm}^2$ and the ratio of the bend mean radius of the curvature R_c to the hydraulic diameter D_h is $R_c/D_h = 3.35$. Both tangents are 31 hydraulic diameters long, and they are attached to the 0 deg (inlet) and 180 deg (outlet) planes of bend by means of flanges, respectively. In Fig.1, X_1, X_2 and X_3 are the coordinates along the streamwise, the spanwise and the vertical directions to bottom wall of the straight duct, respectively. U_θ and U_r represent the streamwise and radial velocities in the cylindrical coordinates and $\overline{u_\theta^2}$ and $\overline{u_r^2}$ are normal stresses corresponding to them, respectively. Reynolds number $Re = U_b D_h/\nu$, where U_b is the bulk mean velocity and ν is the kinematic viscosity of water, was set to 5.67×10^4 and the Dean number De is 2.19×10^4 in the bend. Highly accurate measurement was carried out in developing turbulent flow by making use of laser-Doppler anemometer [4].

2.2 Numerical Schemes

For the modeling of the convective term and of the diffusion term, the approximation by Rodi [8] was employed. Following Chou [9], the pressure-strain model is made. Here we made use of the forth-order tensor presented by Launder, Reece and Rodi [10]. Authors [11] described the derivation of these terms in detail.

The boundary-fitted coordinate system (BFC) was adopted in this present research. The governing equations are discretized by finite differential method with non-staggered computational grid. The QUICK(quadratic interpolation for convective kinematics) approximation of Leonard [16] is used for discretizing convective transport term and the other terms are discretized by central-difference scheme. In numerical solution, implicit method is adopted and successive over relaxation method is utilized as a solution of the algebraic equations.

The detailed procedure has been described by the author's other reports [11] [14] [15].

2.3 Numerical Analysis

Numerical analysis has been performed for Reynolds number $Re = 5.67\times10^4$ which is same as the experiment referred [4]. An inlet and outlet straight ducts, 31 hydraulic diameters long, are also considered as a computational domain together with the curved duct section. Judging from the symmetry of square duct, we set computational domain on the region covered with oblique lines in Fig.1, which corresponds to a half of the whole cross section. Figure 2 shows the arrangement of the calculation mesh over the curved square bend and ξ, η and ζ represent the coordinate axes in the boundary-fitted coordinate system. All the calculations were carried out on a numerical grid with $144\times41\times21$ nodes in the streamwise, radial and normal directions, respectively. The streamwise spacing inside the bend is 3 degree while that of outlet straight duct increase a geometric progression.

Since the inlet condition of the turbulent energy k and the turbulent dissipation ϵ are unknown from the experimental data, the values of $k = U_b\times10^{-5}$, $\epsilon = k^{3/2}/D_h$ were adopted at the inlet section of straight duct. The streamwise velocity with a constant value is assumed at the inlet. The consistence of the universal velocity distribution at the vicinity of the wall and also the supposition of the local equilibrium lead to the utilization of the law of the wall

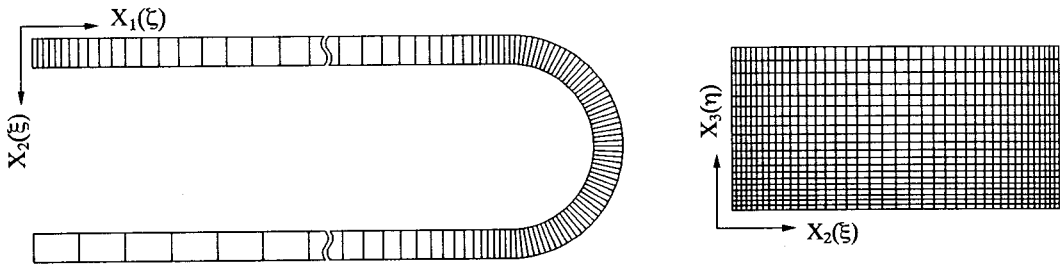

Fig.2: Arrangement of calculation mesh

function as the boundary conditions for k and ϵ equations.

3. RESULTS AND DISCUSSIONS

3.1 Flows in Inlet Straight Duct

The developing turbulent flow in a square duct shows a three-dimensional mean motion resulting from the generation of the turbulence-driven secondary flow. The developing turbulent flow in a square duct is physically complicated contrary to its simple shape. At first, the calculated results which correspond to the 28.3 D_h from the duct inlet and are not affected by the curved bend are compared with the experimental results measured by Melling and Whitelaw [1]. It is noted that their Reynolds number is 4.2×10^4 which is different from te one for this numerical analysis.

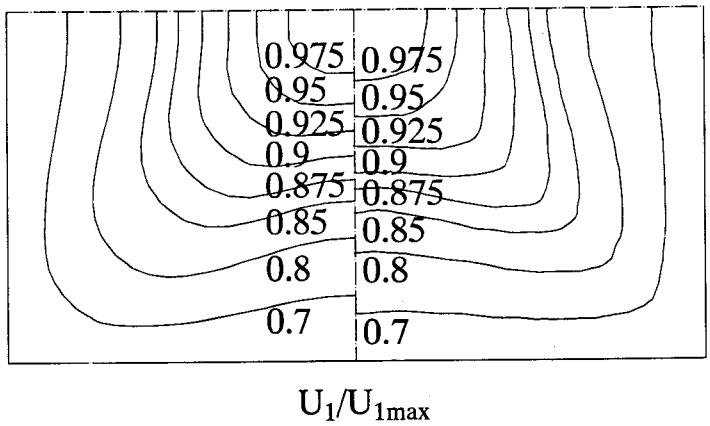

Fig.3: Comparison of streamwise velocity U_1 in straight duct
(Left: Calculated; Right: Exp.[1])

Figures 3 and 4 show the comparison of the calculated contour map of streamwise velocity and velocity vector of secondary flow with the experimental data, respectively. The results of the streamwise velocity is nondimensionalized by the maximum streamwise velocity U_{1max}, which is equivalent to the center mean velocity at this cross section. As shown in Fig.3, both of streamwise velocities present typical bulging towards the corner which is caused by the secondary motion. The vectors of the experiment indicate transport of fluid from the center

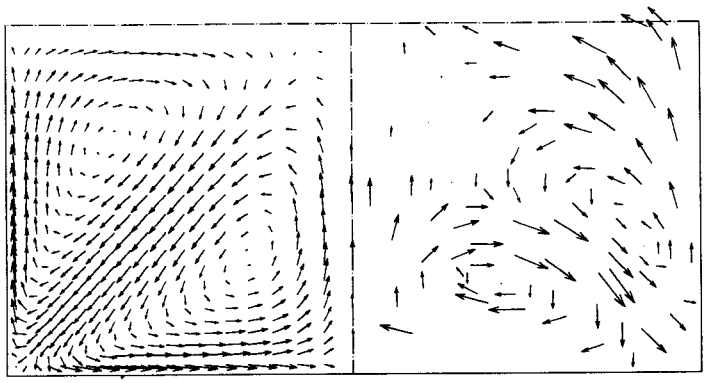

Fig.4: Comparison of secondary flow in straight duct (Left: Calculated; Right: Exp.[1])

towards the corner, then from the corner towards the mid-point of adjacent walls and finally back to the center roughly parallel to the bisectors of the walls. This flow pattern agrees with the calculated results as shown in Fig.4.

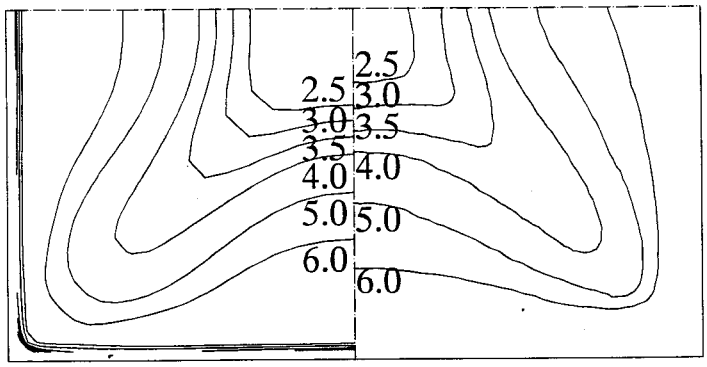

Fig.5: Comparison of turbulent energy in straight duct (Left: Calculated; Right: Exp.[1])

Figure 5 shows the profiles of turbulent energy. The bulging contours of turbulent energy are more stronger towards the corners than one of the mean velocity. The present numerical result also predicts well these characteristic features.

The shear stress $\overline{u_1 u_3}$ is shown in Fig.6. This shear stress is generated by the momentum transfer between the streamwise and the vertical fluctuating velocities. The shear stress component displayes rather complicated behavior than the normal stresses has, i.e. positive and negative regions divided by a zero line are observed. These two different-sign regions occur due to the distorted streamwise velocity caused by the secondary flow. The calculated results are in good agreement with the experimental result as shown in Fig.6.

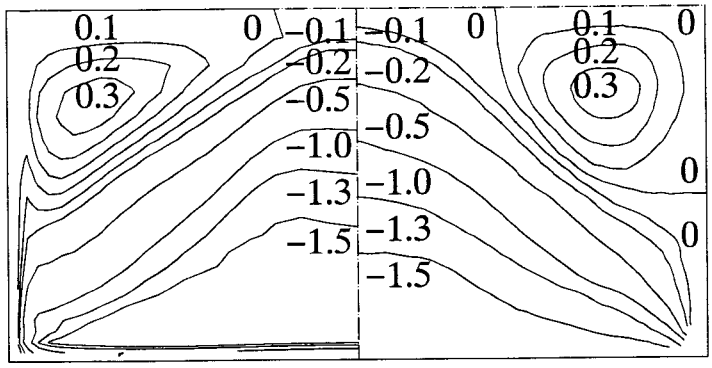

Fig.6: Comparison of shear stress $\overline{u_1 u_3}$ (Left: Calculated; Right: Exp.[1])

3.2 Mean Velocity in Curved Bend

In this section, the numerical results are compared with the experimental results [4] in detail.

The streamwise (U_θ) and radial (U_r) velocity profiles in $x_3 = 0$, -0.25, -0.50, -0.75 and -0.875 planes are shown in Fig.7 $\sim$ 9 at 3 deg, 45 deg and 90 deg bend sections, respectively. Here, x_3 is set as $x_3 = X_3/(D_h/2)$. In 3 deg bend section shown in Fig.7, all the streamwise velocity profiles indicate a maximum point displaced towards the inner wall, due to high pressure near the outer wall. This phenomenon is peculiar to strongly curved ducts. The radial velocity directs everywhere towards the inner wall, except for small regions adjacent to the inner wall and near the symmetry plane. The calculated results are in good agreement with the experimental profiles. As the flow develops, the intensity of the secondary flow grows. At 45 deg bend, the radius velocity U_r near the bottom wall $x_3 = -0.75$, and -0.875 shows a negative value, while at the other x_3 locations they are large and positive. This results suggest that the secondary flow flows from the inner wall to the outer wall along the symmetry plane, and back to the inner wall along the bottom wall of the bend, and that the maximum streamwise velocity is displaced towards the outer wall due to the centrifugal force. These features at 45 deg are well predicted by the present method.

At 90 deg bend section, the experimental results show that a large "hole" develops in the streamwise velocity towards the inside of the bend at $x_3 = 0$ (symmetry plane) and $x_3 = 0.25$ planes as shown in Fig.9. On the other hand, the profiles of the radial velocity also vary remarkably as compared with that of other velocity components. With the present numerical simulation, the large "hole" in the streamwise velocity and the big change of the radial velocity are well reproduced.

Several researchers [5, 6] have tried to predict numerically this large "hole" in the streamwise velocity using turbulent models but agreement with the experiment is far from satisfactory.

Figure 10 shows the contour map of the streamwise velocity and the secondary flow vector diagram at 90 deg bend, and that a strong pressure-driven secondary flow transports the low-velocity fluid from the inner wall region towards the bend center plane, resulting in generation of the large "hole" in the streamwise velocity observed in $x_3 = 0$ and -0.25 plane. These

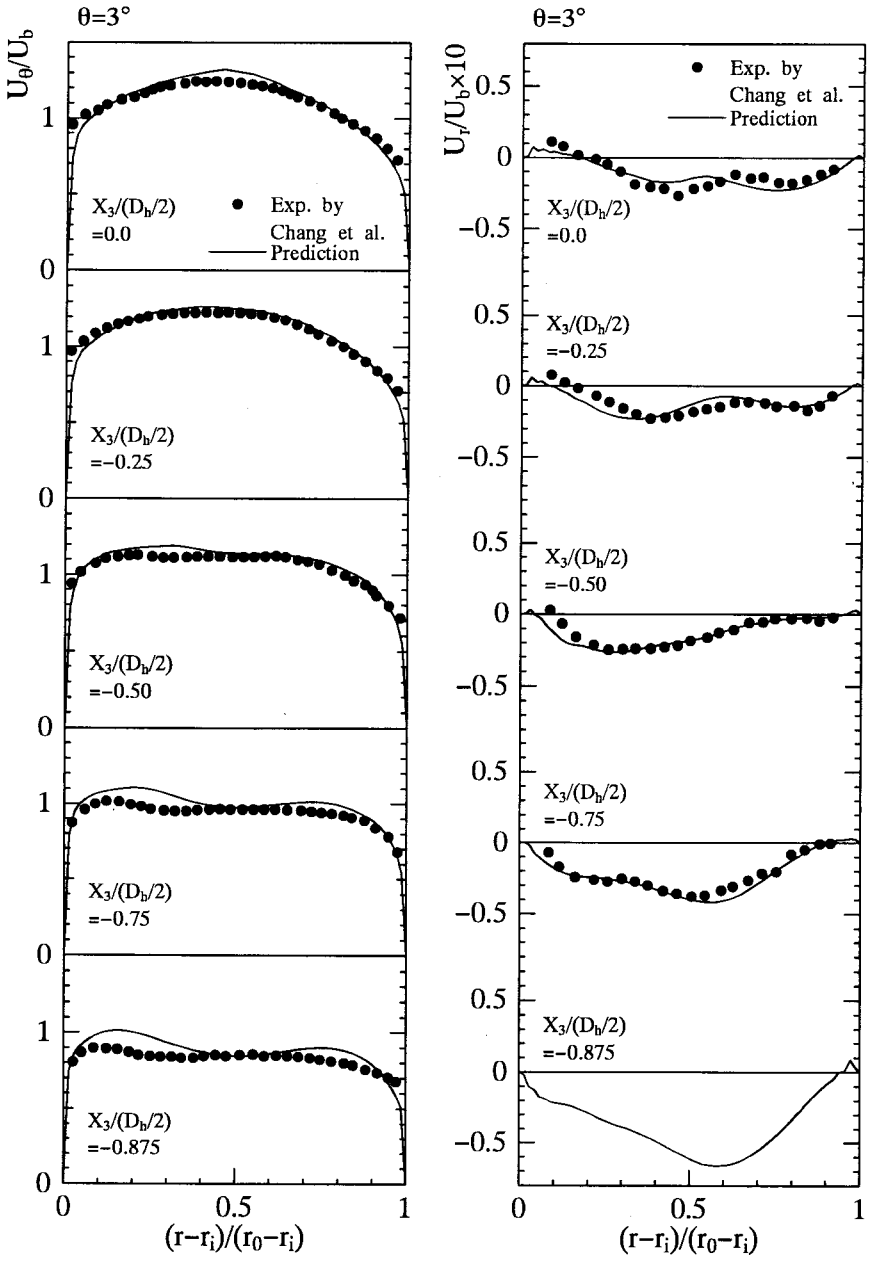

Fig.7: The streamwise U_θ and the radial U_r velocities at 3 deg bend section

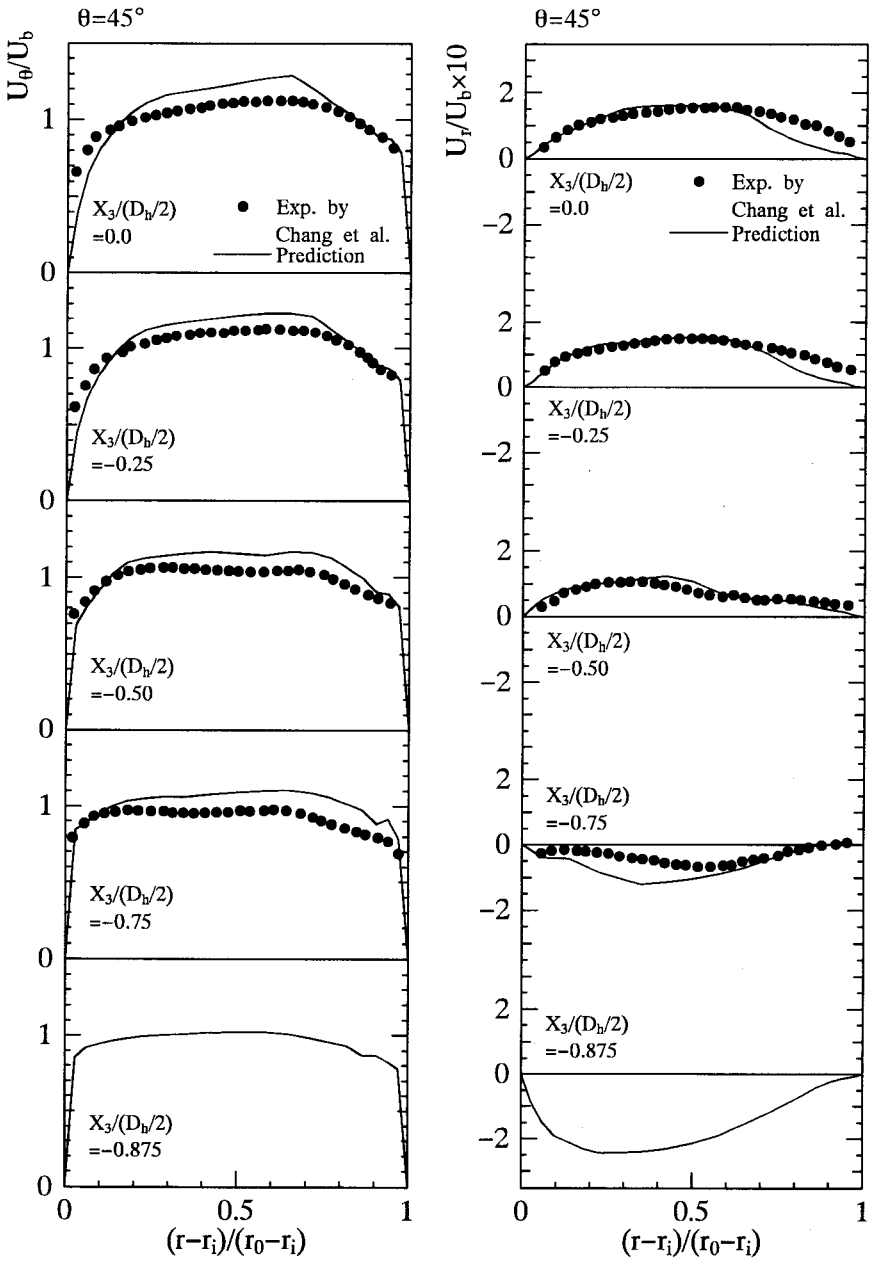

Fig.8: The streamwise U_θ and the radial U_r velocities at 45 deg bend section

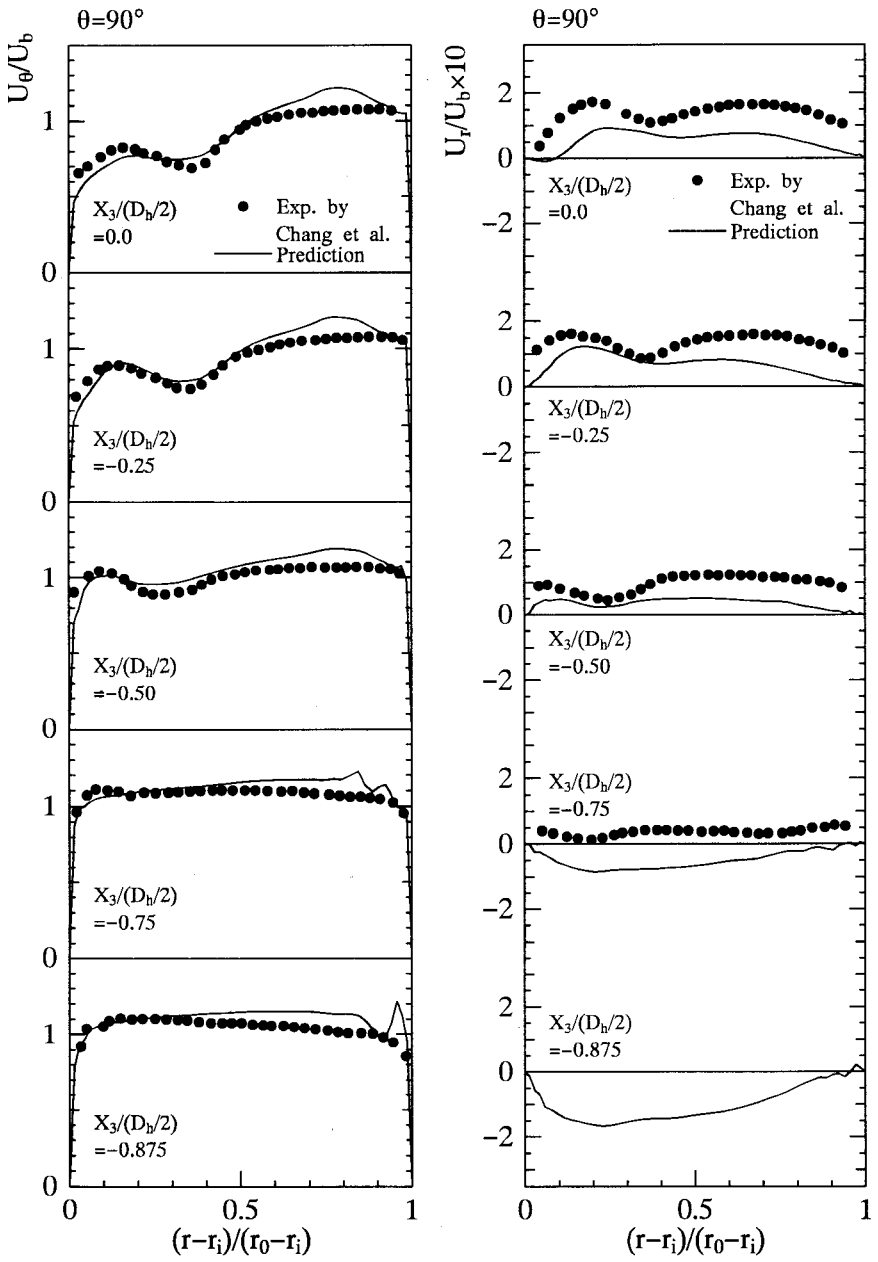

Fig.9: The streamwise U_θ and the radial U_r velocities at 90 deg bend section

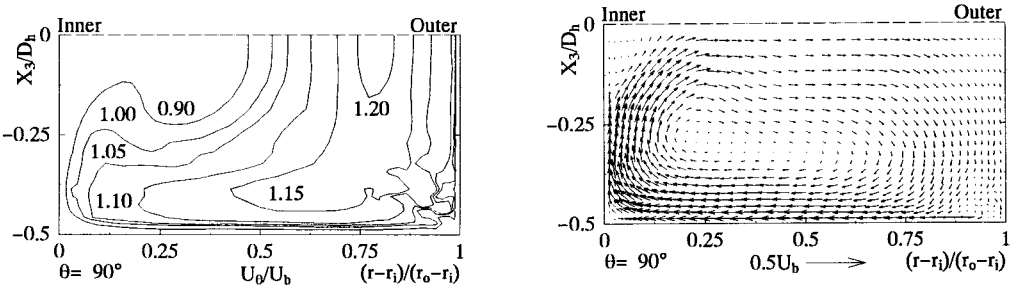

Fig.10: Calculated streamwise U_θ velocity and secondary flow

calculated results suggest that a key factor to simulate correctly the large "hole" is the precise prediction of the secondary flow.

The streamwise and the radial velocities at 177 deg bend section are compared in Fig.11. At this location, the numerical as well as the experimental results show that the large "hole" in the streamwise velocity disappears and the maximum streamwise velocity is displaced towards the outer wall due to the centrifugal force. The present numerical method has a tendency to underestimate the intensity of the secondary motion, and gives rather uniform profile along the line parallel to the symmetry plane.

3.3 Reynolds Stresses in Curved Bend

Algebraic Reynolds stress model adopted in this numerical analysis provides predictions of the anisotropy turbulence as well as the mean velocity components. In Figs.12 $\sim$ 14, the rms streamwise and radial fluctuating velocity profiles are shown at 3, 45 and 90 deg bend sections along the lines parallel to the symmetry plane. The corresponding mean velocity profiles are in Figs.7 $\sim$ 9, respectively. At 3 deg bend section, the calculated both fluctuating velocities are in good agreement with the experiment as seen in Fig.12. The streamwise normal stress indicates the peak value near the inner and outer walls and the radial normal stress decays towards the both walls.

Figure 13 suggests that the distributions of the normal stresses in 45 deg bend becomes more complicate than the case of 3 deg bend owing to production of the strong secondary motion as the flow develops into the bend. Large discrepancy between the numerical and the experimental results observed in this case is probably due to that the present method overestimates the streamwise normal stress near the inner wall, especially at $x_3 = 0$ (symmetry plane) and -0.25 planes.

The production term $P_r(\overline{u_\theta^2})$ of streamwise normal stress is written as

$$P_r(\overline{u_\theta^2}) = -2\overline{u_\theta u_r}\frac{\partial U_\theta}{\partial r} - \frac{2\overline{u_\theta^2}}{r}\frac{\partial U_\theta}{\partial \theta} - \frac{2\overline{u_\theta^2}U_r}{r} - 2\overline{u_\theta u_z}\frac{\partial U_\theta}{\partial z} \qquad (1)$$

At the first term of right hand side, the shear stress $\overline{u_\theta u_r}$ is small near the inner wall as compared with that of the streamwise normal stress $\overline{u_\theta^2}$ and the radial velocity U_r is also lower about one order of magnitude compared to that of the streamwise velocity U_θ. Furthermore, the forth term of right hand side becomes to zero near the symmetry plane. Therefore, the second term

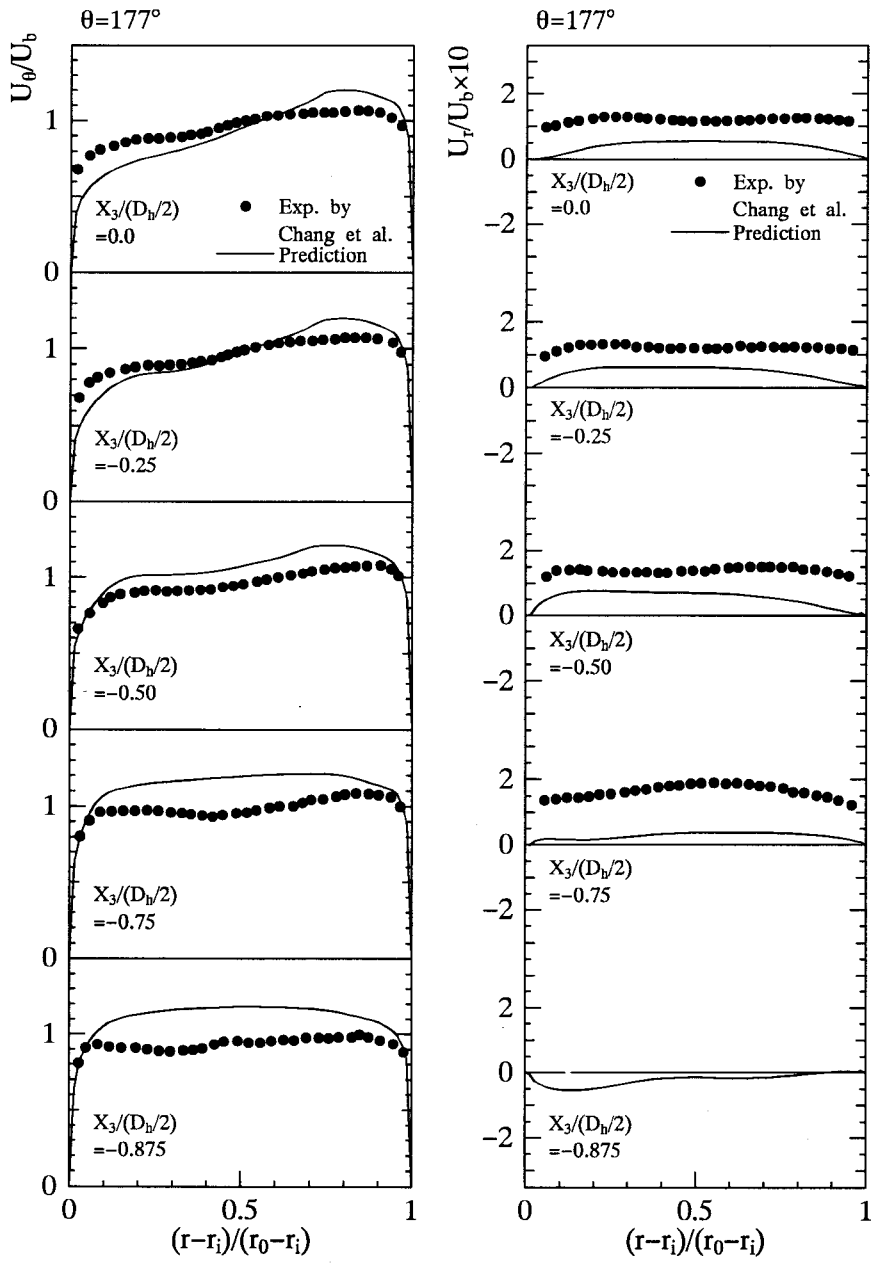

Fig.11: The streamwise U_θ and the radial U_r velocity distributions at 177 deg bend section

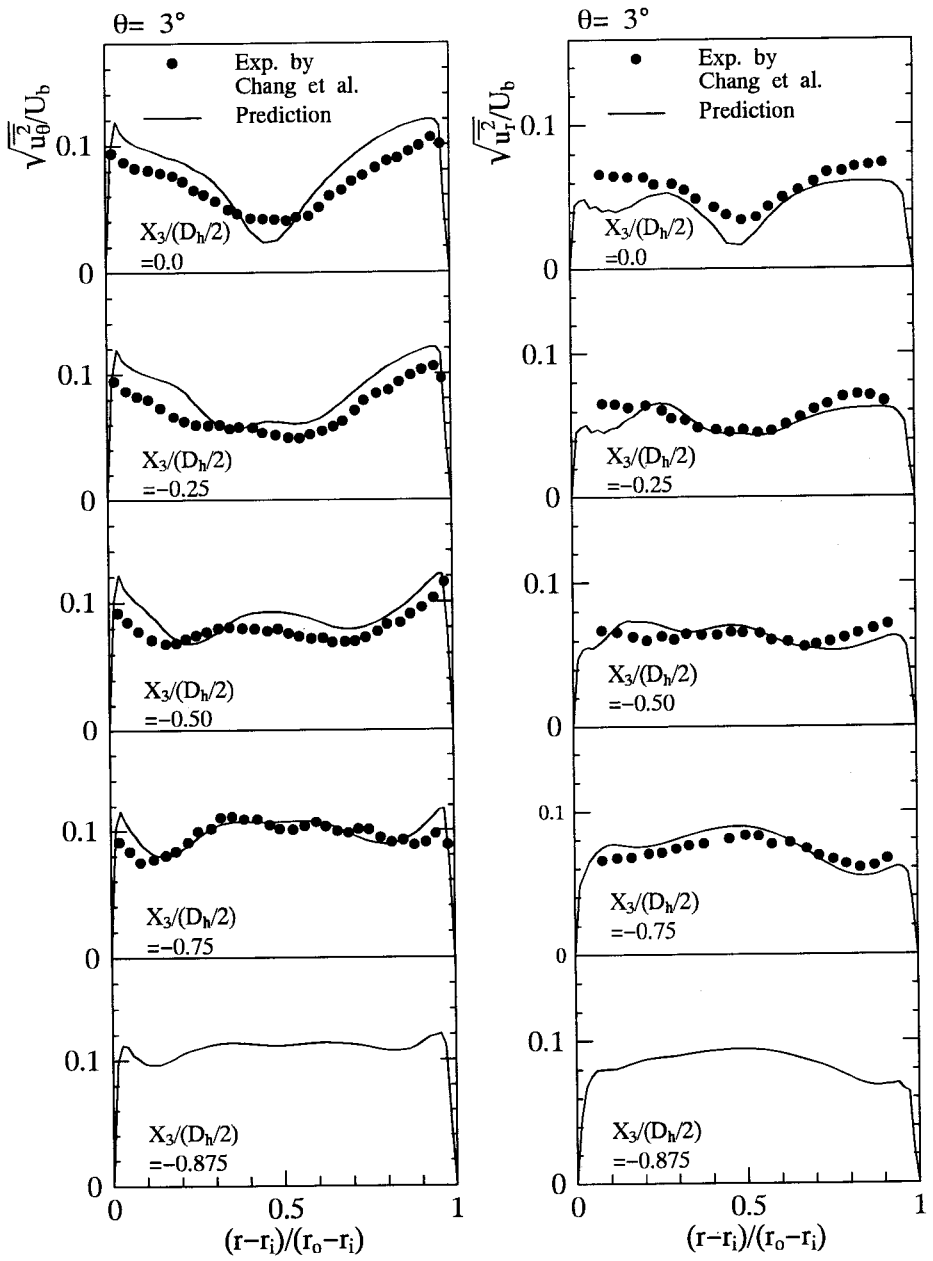

Fig.12: The streamwise $\overline{u_\theta^2}$ and radial $\overline{u_r^2}$ normal stresses at 3 deg bend section

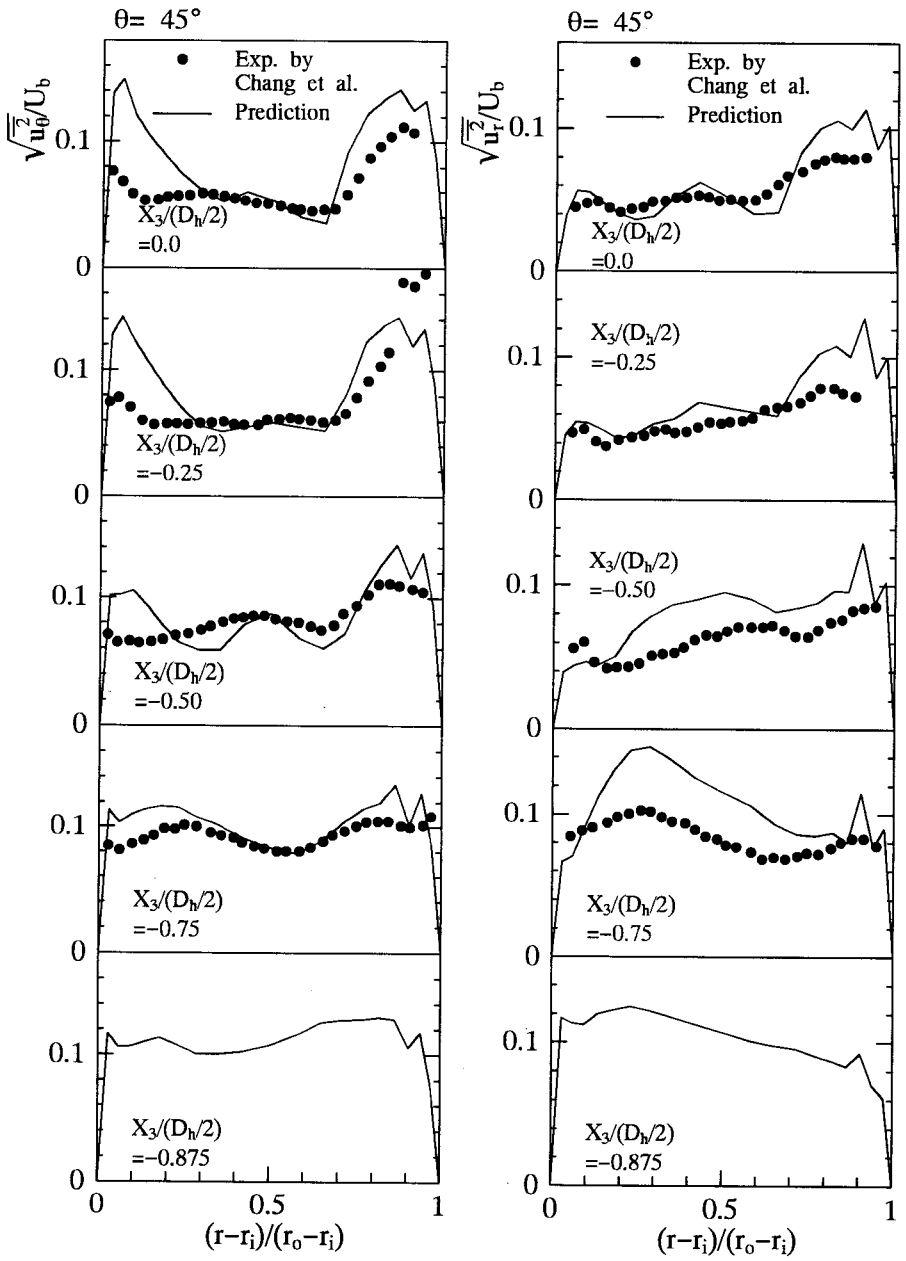

Fig.13: The streamwise $\overline{u_\theta^2}$ and radial $\overline{u_r^2}$ normal stresses at 45 deg bend section

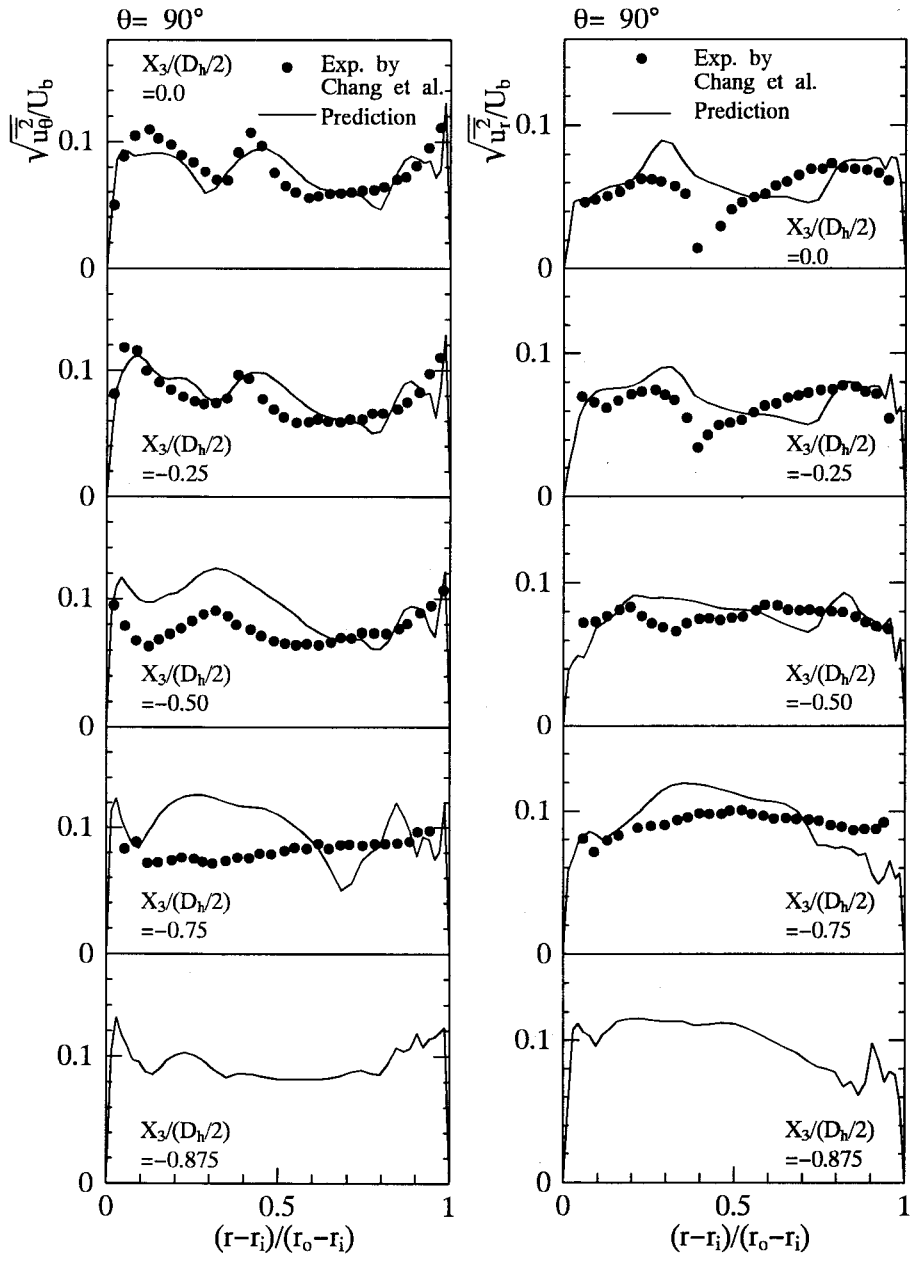

Fig.14: The streamwise $\overline{u_\theta^2}$ and radial $\overline{u_r^2}$ normal stresses at 90 deg bend section

of the right hand side plays an important role with production of streamwise normal stress. At 45 deg bend section, the fluid with low streamwise velocity is transferred from the inner wall to the symmetry plane by strong secondary motion as seen in Fig.8. This transfer of the slow fluid causes the second term to have the minus value for the derivative of streamwise velocity(U_θ) with respect to bend angle. As a result of this minus value, the second term of the production increases its value near the inner wall for the calculated result.

As shown in Fig.14, at 90 deg bend section the experimental plots of the two normal stresses show steep variations in the vicinity of the symmetry plane. These variations of normal stresses are bound up with the profiles of the streamwise and radial mean velocities shown in Fig.9. The present method predict well the profile of streamwise normal stress $\overline{u_\theta^2}$ with steep variation but fails to predict the local decrease of the radial normal stress $\overline{u_r^2}$. The production term $P_r(\overline{u_r^2})$ of radial normal stress is defined as

$$P_r(\overline{u_r^2}) = -2\overline{u_r^2}\frac{\partial U_r}{\partial r} - \frac{2\overline{u_\theta u_r}}{r}\frac{\partial U_r}{\partial \theta} + \frac{2\overline{u_\theta u_r}U_\theta}{r} - 2\overline{u_r u_z}\frac{\partial U_r}{\partial z} \qquad (2)$$

This equation is applied to the region at $R = 0.4$, $(R = (r - r_i)/(r_0 - r_i))$ of the symmetry plane. The derivative of radial mean velocity U_r with respect to the radial coordinate r of the first term changes its sign across the point of $R = 0.4$, i.e. its value decreases with negative sign as approaching the point $R = 0.4$ and, on the contrary, its value increases with positive sign as leaving from that point. These explanations are clear from the profile of the radial mean velocity as shown Fig.9. The shear stress $\overline{u_\theta u_r}$ shows a small value with negative sign. Moreover, the derivative of radial velocity U_r with respect to bend angle is estimated to be negative from the calculated results. Considering these results, we can find that the second and third terms of the right hand side contribute to negative production of the radial normal stress and the derivative U_r with respect to the bend angle in the second term is important factor for local decrease of the radial normal stress. In the light of this fact, the small variation with negative value of the derivative U_r with respect to the bend angle causes the radial normal stress not to decrease remarkably its value near the symmetry plane at $R = 0.4$ in the numerical result.

The distributions of the shear stress $\overline{u_\theta u_r}$ are compared in Fig.15, where the case of 45 deg is shown together with the case of 90 deg bend. The shear stress indicates small value relative to that of the normal stresses and higher value in the vicinity of the outer wall of the symmetry plane at 45 deg bend. The calculated results tend to show negative value near the inner wall and, on the contrary, positive value near the outer wall. This tendency of shear stress results from the positive value near the outer wall and the negative value near the outer wall of the term $-\overline{u_r^2}(\partial U_\theta/\partial r)$ which has a great influence upon production of shear stress. This means that the derivative of the streamwise mean velocity U_θ with respect to radial coordinate r has negative value near the outer wall and positive value near the inner wall.

3.4 Transition of Secondary Flow

The turbulent flow in a strongly curved bend with inlet and outlet tangents presents an interesting phenomenon, i.e. transition from the secondary flow of the second kind to that of the first kind near the inlet of curved bend and vice versa near the outlet of it. In curved duct,

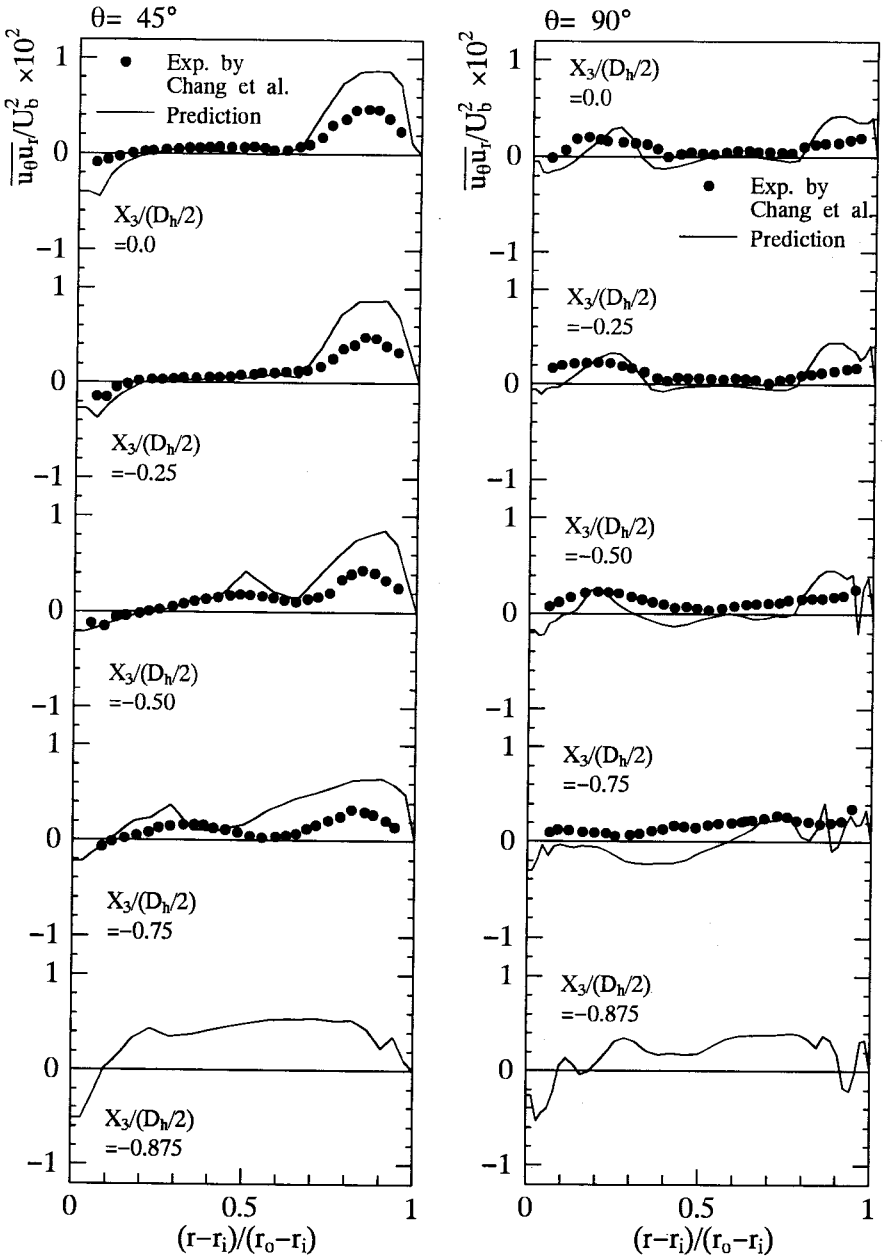

Fig.15: The shear stress $\overline{u_\theta u_r}$ at 45 and 90 deg bend sections

where the centrifugal force acts vertically to the main flow directions, this motion is pressure-induced and is said to be the secondary flow of the first kind. The secondary flow of the second kind is encountered in non-circular straight ducts and it is caused by anisotropy of turbulence. Although there are many reports concerning such flows based on numerical analysis using many kinds of turbulent model, to our knowledge, we can not find any reports refering to the transition of the secondary flow. Therefore, the transition of the secondary flow is examined by using the calculated results to make its behavior clear.

Figures 16 and 17 show the calculated results for the transition of the secondary flow near the inlet and the outlet of the curved duct, respectively. Contours of pressure are presented on right-hand side of these figures, together with the secondary flow vectors on left. At the location $x_1 = -2.3$ ($x_1 = X_1/D_h$), the both distributions of the secondary velocity and the pressure persist the symmetrical form with respect to the vertical center plane. As the flow develops further downstream, the distribution of the pressure destroys its symmetricity as illustrated at $x_1 = -1.0$ owing to the influence of the bend inlet while the secondary flows hold its symmetricity. This phenomenon suggests that the secondary flow is controlled by the anisotropy of turbulence rather than the pressure gradient at this location. In contrast, the turbulence-driven motion is about to transform to the pressure-driven secondary motion at $x_1 = 0.6$ ahead of the bend entry. This transformation of the secondary flow is accelerated at further downstream by increasing the pressure gradient as indicated at $x_1 = -0.2$, where the secondary flow is generated from the outer wall towards the inner wall and its flow pattern is typical one observed near the bend entry. Considering these results, we can say that the precise prediction of the secondary flow in straight duct is the one of major factors to understand satisfactorily the turbulent structure of the bend flow, because the secondary flow of the straight duct has strong influence upon the developing secondary motions in the curved duct.

Figure 17 shows the calculated secondary flow vectors and pressure distributions near the bend outlet. At $0.2D_h$ downstream from the bend outlet, the secondary flow produced by the centrifugal force exists in the similar form as of curved duct. At $X_1 = 2.3D_h$, the secondary flow pattern changes greatly and extends over the half of the cross section as a result of increasing intensity. This acceleration is attributed to the pressure distribution as shown on the right-hand side, i.e. the high pressure near the corner of the inner wall accelerates the secondary flow and simultaneously results in deceleration of the streamwise mean velocity through the adverse pressure gradient along the streamline. The secondary flow in the outlet tangent is characterized by this acceleration effect. After this acceleration, the secondary flow decays and transforms from the first kind to the second kind, as the flow develops further downstream as seen at $X_1 = 5.0D_h$ and $6.5D_h$. At $X_1 = 6.5D_h$, the secondary flow towards the corner, which is typical feature of the turbulence-driven secondary motion, is observed clearly. At further downstream $X_1 = 8.1D_h$, both of the secondary flow and the pressure distribution form the symmetrical pattern with respect to vertical center plane. However, the secondary flow pattern at this cross section is different from that of the inlet straight duct concerning to the symmetry form with respect to the corner bisector. This imbalance of symmetry exists also at further downstream $X_1 = 20D_h$. Therefore, these results may suggest that longer tangent duct is necessary in order to recover fully developed secondary flows.

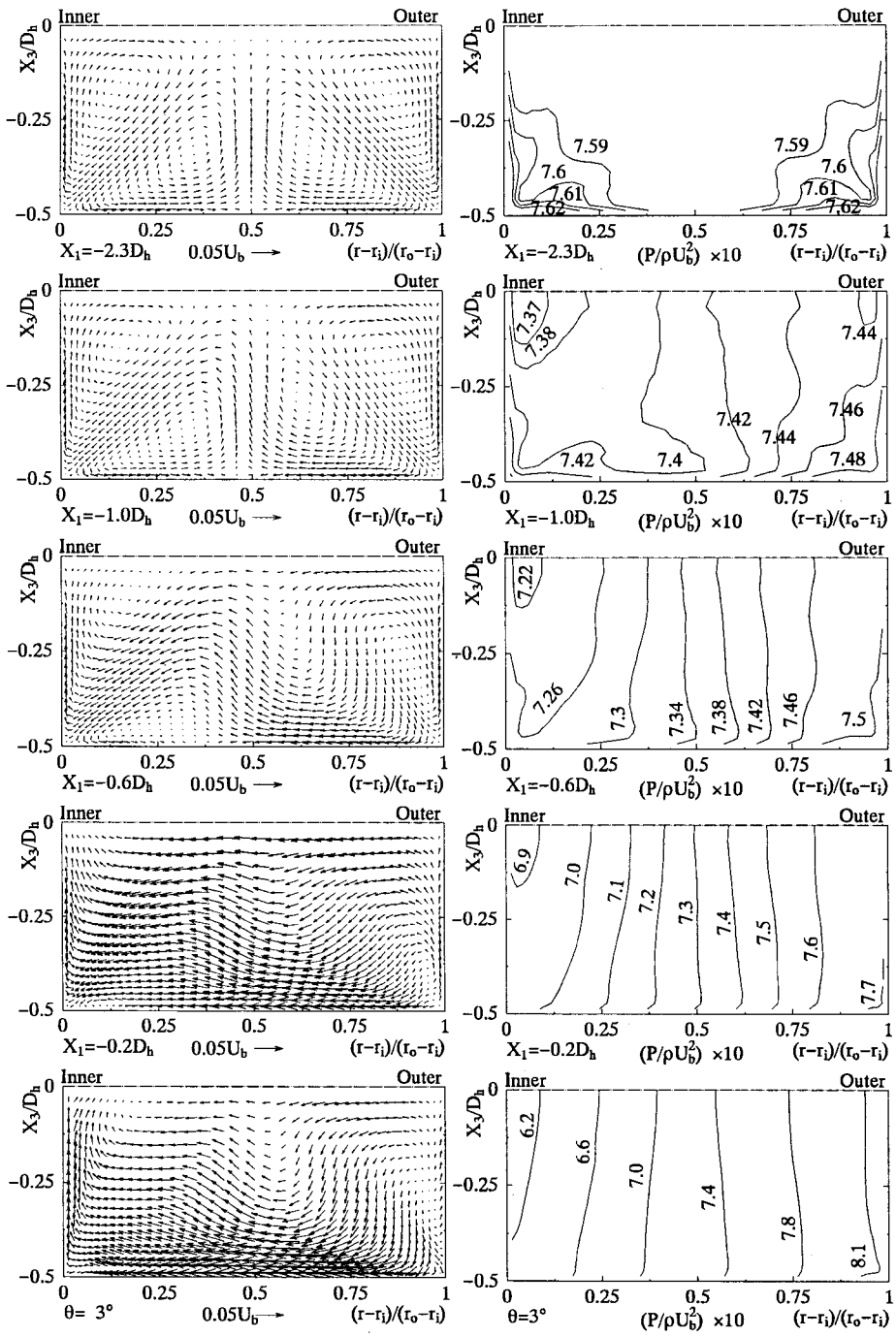

Fig.16: Transition of secondary flow near the bend inlet

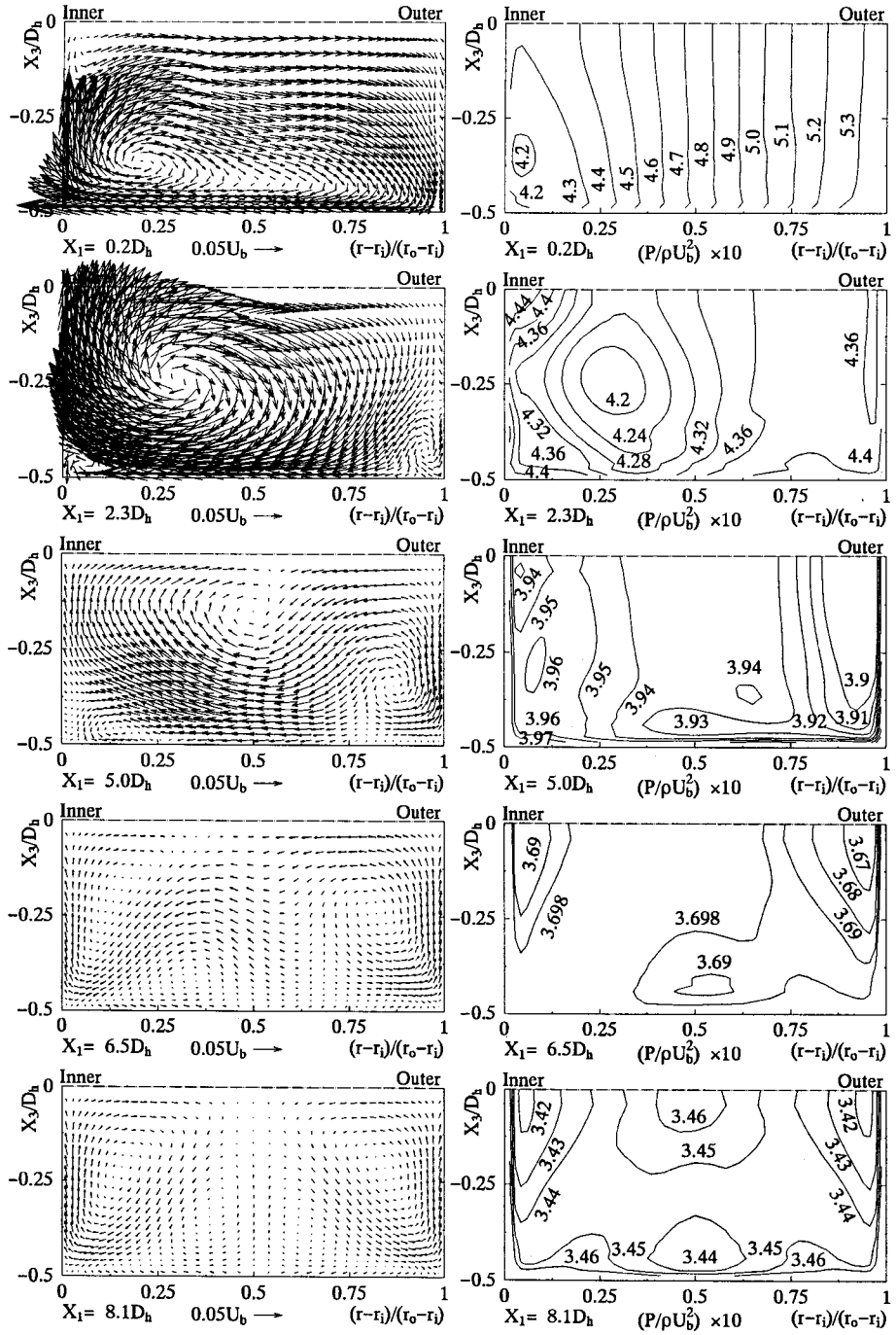

Fig.17: Transition of secondary flow near the bend outlet

4. CONCLUSIONS

Numerical analysis has been carried out for developing turbulent flow in a 180 deg curved duct of square cross section with a bend radius equal to 3.35 times hydraulic diameter of the duct provided with the inlet and outlet tangents. The transition from the turbulence-driven secondary flow to the pressure-driven secondary flow in the inlet tangent and vise versa in the outlet tangent are simulated successfully, which are very interesting to researchers. In order to predict preciously these two kinds of the secondary flow and anisotropy turbulence of the curved duct, algebraic Reynolds stress model coupled with boundary-fitted coordinate system is adopted in this study. The calculated results are compared with two kinds of the experimental data available [1] and [4] to confirm the validity of the present method. Then the transition mechanism of the secondary flow is examined using calculated data to provide insights into its transition.

The calculated mean velocity and Reynolds stresses in the inlet straight duct are in good agreement with the experimental data [1], showing the distorted contour lines of the streamwise velocity and the turbulent energy induced by the turbulence-driven secondary flow. In comparison with the other numerical analysis, the present method can predict well profiles of the streamwise and the radial mean velocity. Displacement of the maximum streamwise velocity along the symmetry plane from the inner wall towards the outer wall between 3 deg and 45 deg bend sections and forming of a large "hole" in the streamwise mean velocity distribution at 90 deg bend section are reproduced well by the present method. Moreover, the calculated profiles of the Reynolds stresses give very similar distributions to the experimental profiles. Although considerably low radial normal stress is numerically observed at 90 deg bend along the symmetry plane.

The transition from the turbulence-driven secondary flow to the pressure-driven one takes place at about $1.0 \sim 0.6\, D_h$ ahead of the bend inlet. On the other hand, the opposite transition near the bend outlet is observed at about $6.5\, D_h$ downstream from the bend outlet after the secondary flow is accelerated due to increasing pressure gradient.

REFERENCES

[1] A.Melling and J.H.Whitelaw (1976) Turbulent flow in a rectangular duct; J. Fluid Mech., vol.78 pp.289–315

[2] A.C.Humphrey, J.H.Whitelaw and G.Yee (1981) Turbulent flow in a square duct with strong curvature; J. Fluid Mech., vol.103 pp.443–463

[3] A.M.K.P.Taylor, J.H.Whitelaw and M.Yianneskis (1982) Curved ducts with strong secondary motion:velocity measurements of developing laminar and turbulent flow; Trans. ASME, J. Fluids Eng., vol.104 pp.350–359

[4] S.M.Chang, J.A.C.Humphrey and A.Modavi (1983) Turbulent flow in a strongly curved U-bend and downstream tangent of square cross-sections; PHC Physico Chemical Hydrodynamics,vol.4 no.3 pp.243–269

[5] Y.D.Choi, H.Iacovides and B.E.Launder (1989) Numerical computation of turbulent flow in a square-sectioned 180 deg bend; Trans. ASME, J. Fluids Eng., vol.111 pp.59–68

[6] F.Sotiropoulos and V.C.Patel (1993) Evaluation of some near-wall models for the

Reynolds-stress transport equations in a complex 3-D shear flow; *Near-Wall Turbulent Flows*, Elsevier Science Publishers, pp.987–997

[7] B.E.Launder and N.Shima (1989) Second-moment closure for the near-wall sublayer:development and application; AIAA Journal, vol.27 pp.1319–1325

[8] W. Rodi (1976) A new algebraic relation for calculating the Reynolds stresses; Z. Angew. Math. Mech., vol.56 pp.T219–T221

[9] P.Y.Chou (1945) On velocity correlations and the solutions of the equations of turbulent fluctuation; Quart. Appl. Math., vol.3 pp.38–54

[10] B.E.Launder, G.J.Reece and W.Rodi (1975) Progress in the development of a Reynolds stress turbulence closure; J. Fluid Mech., vol.68 pp.537–566

[11] H.Sugiyama, M.Akiyama, M.Matsumoto, M.Hirata, and N.Ninomiya (1993) Numerical analysis of fully developed turbulent flow in a square duct with two facing roughened walls; CFD Journal, vol.2 pp.319–338

[12] F.H.Champagne, V.G.Harris, and S.Corrsin (1970) Experiments on nearly homogeneous turbulent shear flow; J. Fluid Mech., vol.41 pp.81–139

[13] V.G.Harris, J.A.H.Graham, and S.Corrsin (1977) Further experiments in nearly homogeneous turbulent shear flow; J. Fluid Mech., vol.81 pp.657–687

[14] H.Sugiyama, M.Akiyama, K.Yamanaka and M.Hirata (1995) Numerical analysis of turbulent structure in a rectangular duct with sand ridges; CFD Journal, vol.4 pp.59–78

[15] H.Sugiyama, M.Akiyama, T.Matsubara and m.Hirata (1995) Numerical analysis of three-dimensional turbulent strucutre in open channel flow; CFD Journal, vol.4 pp.239–264

[16] B.P.Leonard (1979) A stable and accurate convective modelling procedure based on quadratic upstream interpolation; Comp. Meths. Appl. Mech. Eng., vol.19 pp.59–98

[17] M.M.Gibson and B.E.Launder (1976) On the calculation of horizontal, turbulent, free shear flows under gravitational influence; Trans. ASME, J. Heat Trans., vol.98 pp.81–87

[18] M.Akiyama, H.Kawamura, T.Serizawa, H.Sugiyama, T.Kunugi and I.Nishiwaki (1889) An algebraic stress model analysis of fully developed turbulent flow in a square duct; Trans. JSME, vol.55 pp.351–357 (in Japanese)

[19] Report of benchmark from CFD codes, RC104, JSME, May 20, 1994 (in Japanese)

[20] C.L.Freitas (1995) *Perspective: Selected benchmarks from commercial CFD codes*; Trans. ASME, vol.117 pp.208–218